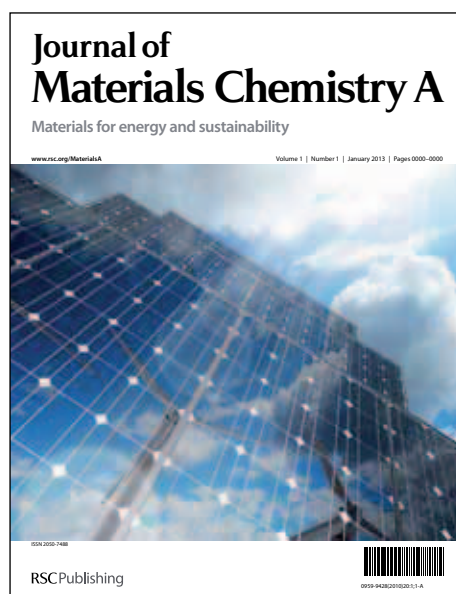


# Journal of Materials Chemistry A

Accepted Manuscript



This is an *Accepted Manuscript*, which has been through the RSC Publishing peer review process and has been accepted for publication.

*Accepted Manuscripts* are published online shortly after acceptance, which is prior to technical editing, formatting and proof reading. This free service from RSC Publishing allows authors to make their results available to the community, in citable form, before publication of the edited article. This *Accepted Manuscript* will be replaced by the edited and formatted *Advance Article* as soon as this is available.

To cite this manuscript please use its permanent Digital Object Identifier (DOI®), which is identical for all formats of publication.

More information about *Accepted Manuscripts* can be found in the [Information for Authors](#).

Please note that technical editing may introduce minor changes to the text and/or graphics contained in the manuscript submitted by the author(s) which may alter content, and that the standard [Terms & Conditions](#) and the [ethical guidelines](#) that apply to the journal are still applicable. In no event shall the RSC be held responsible for any errors or omissions in these *Accepted Manuscript* manuscripts or any consequences arising from the use of any information contained in them.

Cite this: DOI: 10.1039/c0xx00000x

ARTICLE TYPE

www.rsc.org/xxxxxx

## Hierarchical Core-Shell $\alpha$ -Fe<sub>2</sub>O<sub>3</sub>@C Nanotubes as a High-Rate and Long-life Anode for Advanced Lithium Ion Batteries

Xin Gu,<sup>a</sup> Liang Chen,<sup>a</sup> Shuo Liu,<sup>a</sup> Huayun Xu,<sup>a</sup> Jian Yang<sup>\*a</sup>, and Yitai Qian<sup>ab</sup>

Received (in XXX, XXX) XthXXXXXXXXXX 20XX, Accepted Xth XXXXXXXXXXXX 20XX

DOI: 10.1039/b000000x

High-performance anode materials in lithium ion batteries greatly lie on the elaborate controls on their size, shape, structure and surface. However, it is difficult to assemble all the controls within one particle, due to difficulties in synthesis. Here, hierarchical carbon-coated  $\alpha$ -Fe<sub>2</sub>O<sub>3</sub> nanotubes are prepared by a facile hydrothermal reaction between branched MnO<sub>2</sub>/Fe<sub>2</sub>O<sub>3</sub> nanorods and glucose. The resulting nanotubes realize all these controls in one particle in terms of nanoscale size, one-dimensional shape, hollow structure, hierarchical surface and carbon coating. Meanwhile, the thickness of the carbon layer could be easily controlled by the ratio between different reactants. Electrochemical measurements show that the core-shell nanotubes with a thinnest carbon layer give the best cycling and rate performances. They deliver a specific capacity of 1173 mAh g<sup>-1</sup> after 100 cycles at a current density of 0.2 A g<sup>-1</sup>, or 1012 mAh g<sup>-1</sup> after 300 cycles at 1 A g<sup>-1</sup>. Even after 1000 cycles at a current density of 4 A g<sup>-1</sup>, the specific capacity could be still kept at 482 mAh g<sup>-1</sup>. The excellent lithium-storage performances could be attributed to the well-designed controls in this nanocomposite and a thin carbon layer that increase the electron conductivity of the electrode and keep the carbon content lower simultaneously.

### Introduction

In the past few years, rechargeable lithium-ion batteries (LIBs) have attracted extensive attention, due to their excellent performances in portable electronics, electric vehicles (EVs) and hybrid electric vehicles (HEVs).<sup>1, 2</sup> Traditional graphite anode in LIBs that exhibits a low theoretical capacity of 372 mAh g<sup>-1</sup> and faces a severe safety problem as well, cannot meet the needs in terms of specific capacity and power density. So, transition metal oxides (*e.g.*, MnO, Fe<sub>2</sub>O<sub>3</sub>, Co<sub>3</sub>O<sub>4</sub>, *et. al.*) have been developed as a candidate for the anode, in view of large theoretical capacity.<sup>3-5</sup> But they usually show a poor electronic conductivity and a large volume variation during the discharge and charge processes, both of which greatly affect the cycling stability and rate capability. In order to address the issues, some strategies have been realized to improve their performances, including the fabrication of one-dimensional nanomaterials<sup>6, 7</sup> and hollow/porous structures,<sup>8-11</sup> the surface coating of carbon or conductive polymer,<sup>12-15</sup> and the formation of hierarchical surfaces.<sup>4, 12, 16, 17</sup> These controls on the size, shape, surface and structure of the electrode could effectively shorten the diffusion pathway of Li/Li<sup>+</sup>, enhance the electronic conductivity, accommodate the volume change during the discharge/charge processes, and improve the contact between electrolyte and electrode. Although these strategies individually or some of them together have been demonstrated for the anode of LIBs, the ensemble of these strategies into one particle is

seldom reported, because it is difficult to achieve all the controls on the size, shape, surface and structure simultaneously.

Fe<sub>2</sub>O<sub>3</sub>, as a good candidate for anode in lithium ion batteries, has many advantages, such as high theoretical specific capacity, large natural abundance, and low environment contamination. So far, a myriad of Fe<sub>2</sub>O<sub>3</sub> nanostructures have been synthesized and examined as the anode material for lithium ion batteries, including nanorods, nanotubes, porous structures, hollow spheres and their carbon composites.<sup>4, 18-21</sup> In spite of this, the assembly of all the above strategies into Fe<sub>2</sub>O<sub>3</sub> is still a great challenge. Until recently, such a control was demonstrated by the synthesis of carbon-coated hollow  $\alpha$ -Fe<sub>2</sub>O<sub>3</sub> nanohorns grown on carbon nanotubes.<sup>22</sup> The anode based on them delivered a capacity of 800 mAh g<sup>-1</sup> after 100 cycles at 500 mA g<sup>-1</sup>. Their rate capabilities at 1 A g<sup>-1</sup> and 3 A g<sup>-1</sup> were 500 and 420 mAh g<sup>-1</sup>, respectively. Later, the encapsulation of Fe<sub>2</sub>O<sub>3</sub> nanoparticles inside carbon nanotubes was also achieved by a multiple-step process.<sup>23</sup> They exhibited a reversible capacity of 811 mAh g<sup>-1</sup> after 100 cycles at a very low current density of 35 mA g<sup>-1</sup>. The capacity quickly went down to 335 mAh g<sup>-1</sup> at a current density of 1200 mA g<sup>-1</sup> in the rate capability.

Herein, another example to assemble all the controls on size, shape, structure and surface is given by the branched core-shell Fe<sub>2</sub>O<sub>3</sub>@C nanotubes, which combines nanoscale size, one-dimensional shape, hollow structure, surface coating and hierarchical surface together within one particle. The branched nanotubes are

synthesized by a mild hydrothermal reaction between glucose and  $\text{MnO}_2/\text{Fe}_2\text{O}_3$  nanorods. Then, they are characterized by XRD pattern, SEM and TEM images, Raman spectra and TG analysis to reveal its size, shape, structure and components. The thickness of the carbon layer could be easily tailored by the ratio of the reactants. The core-shell nanotubes with different thicknesses of the carbon layer are tested as an anode for lithium ion batteries. It is found that the core-shell nanotubes with a thinnest carbon layer show the best lithium-storage performance. They could maintain a specific capacity of  $1012 \text{ mAh g}^{-1}$  after 300 cycles at  $1 \text{ A g}^{-1}$ . Even after 1000 cycles at  $4 \text{ A g}^{-1}$ , the specific capacity is still kept at  $482 \text{ mAh g}^{-1}$ , higher than commercial graphite. These results demonstrate the benefits of the controls on the electrode.

## Experimental Section

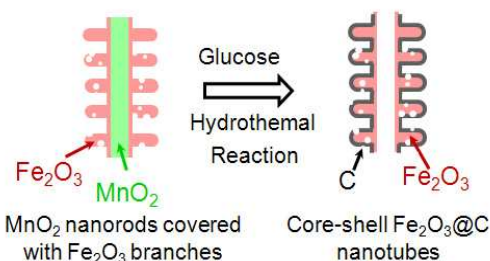
**Synthesis of branched core-shell  $\alpha\text{-Fe}_2\text{O}_3@\text{C}$  nanotubes:** All the reagents were received from Sino-pharm Chemical Reagent Co. Ltd. without further purification. In a typical synthesis, the  $\beta\text{-MnO}_2$  nanorods coated with the  $\alpha\text{-Fe}_2\text{O}_3$  branches were prepared firstly according to our previous work.<sup>24</sup> Then, an appropriate amount of the branched nanorods was dispersed in 10 mL of 1 wt% glucose by ultrasonication. The resulting suspension was transferred into a clean Teflon-lined autoclave and was kept at  $190^\circ\text{C}$  for 5 h. Finally, the branched core-shell  $\alpha\text{-Fe}_2\text{O}_3@\text{C}$  nanotubes were collected by filtration, washed with distilled water and absolute ethanol, and dried in air at  $80^\circ\text{C}$  for the following characterization. In order to identify the effect of the carbon coating on the electrochemical performances, the products with different carbon contents were fabricated by using different ratios of the branched nanorods and glucose. The other experimental conditions were kept as the same. The products obtained with 50, 30 and 20 mg of the branched nanorods were denoted as Sample I, II and III.

**Sample Characterization:** Powder XRD patterns were achieved on an advanced X-ray diffractometer (Bruker D8 Adv., Germany), using monochromatic  $\text{Cu-K}\alpha$  line as a radiation source. Field-emission scanning electron microscope (FESEM) images and transmission electron microscope (TEM) images were obtained from a field-emission scanning electron microscope (SUPRA 55 SAPHIRE) and a transmission electron microscope (JEOL JEM 1011), respectively. High-resolution TEM images (HRTEM) were recorded with an analytic transmission electron microscope (JEOL JEM-2100). Raman spectra were acquired from a NEXUS 670 Raman spectrometer using an excitation wavelength of 632 nm. Thermal gravimetric analysis (TGA) was performed on a Mettler Toledo TGA/SDTA851 thermal analyzer in air at a heating rate of  $10^\circ\text{C min}^{-1}$ .

**Electrochemical Measurements:** The working electrode for electrochemical properties was prepared by 70 wt% active material, 20 wt% conductive carbon black and 10 wt% sodium carboxymethyl cellulose (CMC). In the presence of trace water, the above materials were mixed to produce a slurry. Then, the slurry was coated on a copper foil, and dried under vacuum at  $80^\circ\text{C}$  for 12 h. The resulting foil was roll-pressed and cut into discs. The typical loading density of the active materials on the discs was about  $\sim 1 \text{ mg cm}^{-2}$  if no special instructions. After that, a coin-type cell of CR2032 was assembled in an argon-filled

glove box with a lithium foil as the counter electrode, a Celgard 2300 membrane as the separator and a mixture of ethylene carbonate (EC), ethylmethyl carbonate (EMC) and dimethyl carbonate (DMC) (1:1:1, volume ratio) as the electrolyte. Galvanostatic discharge-charge cycling was performed in a voltage range of 0.01–3 V at a current density of  $0.2\text{--}4 \text{ A g}^{-1}$  at room temperature on a lithium battery cyler (LANDCT-2001A, Wuhan, China). The mass capacity values are calculated based on the composite.

## Results and Discussion



**Scheme 1** Synthesis of branched core-shell  $\text{Fe}_2\text{O}_3@\text{C}$  nanotubes.

The branched core-shell  $\alpha\text{-Fe}_2\text{O}_3@\text{C}$  nanotubes were synthesized by a mild hydrothermal reaction between  $\beta\text{-MnO}_2/\alpha\text{-Fe}_2\text{O}_3$  nanorods and glucose, as described in Scheme 1. Fig. 1 presents the XRD pattern, SEM image and TEM image of the branched core-shell nanotubes. All the reflections in the XRD pattern could be indexed as  $\alpha\text{-Fe}_2\text{O}_3$  (JCPDS Card, No. 33-0664). Compared with the XRD pattern of the  $\beta\text{-MnO}_2/\alpha\text{-Fe}_2\text{O}_3$  nanorods used as the reactant (Fig. S1), the signals of  $\text{MnO}_2$  are absent in the pattern, indicating its disappearance from the product. This result is confirmed by TEM images and EDS spectra (Fig. S2). The SEM image shows the branch-like feature of the core-shell  $\alpha\text{-Fe}_2\text{O}_3@\text{C}$  nanotubes highlighted by red in the inset. It is believed that this feature inherits from the  $\beta\text{-MnO}_2/\alpha\text{-Fe}_2\text{O}_3$  nanorods (Fig. S3). Besides, a few carbon particles appear in the product, as indicated by the arrows. The TEM image reveals the hollow structure located along the axial direction, where is supposed to be  $\text{MnO}_2$  in the case of  $\beta\text{-MnO}_2/\alpha\text{-Fe}_2\text{O}_3$  nanorods. The diameter

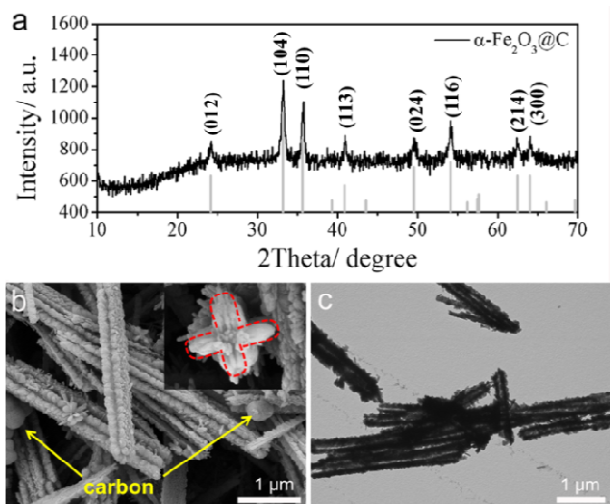


**Fig. 1** (a) XRD patterns, (b) SEM image and (c) TEM image for branched core-shell  $\alpha\text{-Fe}_2\text{O}_3@\text{C}$  nanotubes.

of the hollow structure is around  $\sim 150$  nm, also consistent with that of  $\text{MnO}_2$  in the  $\beta\text{-MnO}_2/\alpha\text{-Fe}_2\text{O}_3$  nanorods. All these results indicate the removal of  $\text{MnO}_2$  from the  $\beta\text{-MnO}_2/\alpha\text{-Fe}_2\text{O}_3$  nanorods after the reaction, resulting in the formation of the branched nanotubes. This removal of  $\text{MnO}_2$  comes from the redox reaction between  $\text{MnO}_2$  and glucose, which leads to the reduction of  $\text{MnO}_2$  to  $\text{Mn}^{2+}$  and then the diffusion into the solution. Meanwhile, glucose decomposes to carbon deposited on the surface of the nanotubes,<sup>25</sup> which is confirmed by the HRTEM image, TGA analysis and Raman spectra.

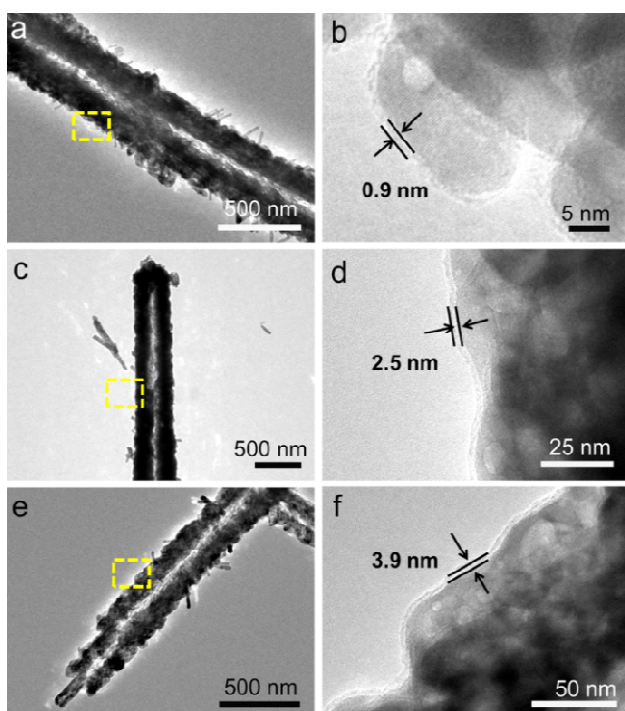


**Fig. 2** TEM and HRTEM images of branched core-shell  $\alpha\text{-Fe}_2\text{O}_3/\text{C}$  nanotubes with the carbon layers in different thicknesses. (a, b) Sample I, Carbon layer: 0.9 nm (c, d) Sample II, Carbon layer: 2.5 nm, and (e, f) Sample III, Carbon layer: 3.9 nm.

A set of TEM and HRTEM images of the branched nanotubes is shown in Fig. 2a and 2b. The HRTEM image of the enclosed area on the surface, directly presents the uniform coating of the carbon layer and the porous structure of  $\text{Fe}_2\text{O}_3$  for the nanotubes. The thickness of the carbon layer could be controlled by the variation of the ratio between the  $\beta\text{-MnO}_2/\alpha\text{-Fe}_2\text{O}_3$  nanorods and glucose, which has been verified by the products obtained by different amounts of the  $\beta\text{-MnO}_2/\alpha\text{-Fe}_2\text{O}_3$  nanorods and a fixed amount of glucose. As described in Fig. 2, the branched nanotubes prepared by 50, 30 and 20 mg of  $\beta\text{-MnO}_2/\alpha\text{-Fe}_2\text{O}_3$  nanorods, denoted as Sample I, II and III, exhibit a carbon-layer thickness of 0.9, 2.5 and 3.9 nm, respectively.

The formation of the carbon layer is also supported by Raman spectra and TGA analysis. As shown in Fig. 3a, two peaks at 1380 and 1580  $\text{cm}^{-1}$  are observed for all three samples, which could be attributed to the D and G band of the carbon shell. The increased peak intensities of the peaks from Sample I to Sample III can be associated with the increased thickness of the carbon layer, as examined by HRTEM images. The result is further confirmed by TGA analysis in air at a heating rate of  $10^\circ\text{C min}^{-1}$ .

As shown in Figure 3b, there is a sharp weight loss from 200 to 400  $^\circ\text{C}$  for all three samples.  $\alpha\text{-Fe}_2\text{O}_3$  could be still kept in the product after the heating treatment at 600  $^\circ\text{C}$  in air (Fig. S4), the weight loss here could be assigned to the removal of carbon. The carbon contents based on these weight losses are estimated to be 20, 33 and 39 % for Sample I, II and III, respectively. The high carbon content might come from the carbon layer in  $\alpha\text{-Fe}_2\text{O}_3/\text{C}$  nanotubes and the carbon particles in the product.

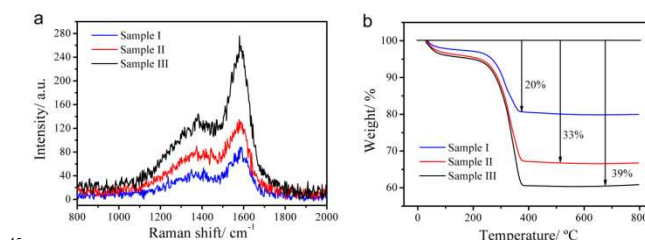


**Fig. 3** (a) Raman spectra and (b) TGA curves of branched core-shell  $\alpha\text{-Fe}_2\text{O}_3/\text{C}$  nanotubes with different thicknesses of the carbon layers.

The uniform surface coating of carbon, the porous structure inside  $\text{Fe}_2\text{O}_3$  branches and the hollow structure of nanotubes, make the composite an excellent candidate as an anode for LIBs. So, the branched core-shell  $\text{Fe}_2\text{O}_3/\text{C}$  nanotubes are evaluated by a half cell of  $\text{Fe}_2\text{O}_3/\text{C}/\text{Li}$ . All the electrochemical measurements are carried out at room temperature between 0.01 and 3.0 V (Vs.  $\text{Li}^+/\text{Li}$ ). Fig. 4a shows the first discharge-charge curves of the nanotubes in different thicknesses. All these curves exhibit the similar profiles. They quickly drop from the open-circuit voltage to  $\sim 0.9$  V first, which could be attributed to the lithium insertion in  $\alpha\text{-Fe}_2\text{O}_3$  to  $\alpha\text{-LiFe}_2\text{O}_3$  and the transformation from  $\alpha\text{-LiFe}_2\text{O}_3$  to cubic  $\text{Li}_x\text{Fe}_2\text{O}_3$ . After that, the curves come with a plateau at  $\sim 0.9$  V, which could be assigned to the complete conversion from  $\text{Li}_x\text{Fe}_2\text{O}_3$  to metallic  $\text{Fe}^0$ . Then, the voltage gradually goes down to 0.01 V, which might be related to the formation of the solid electrolyte interphase (SEI) film on the surface of the electrode.<sup>22, 26</sup> The initial coulombic efficiency of Sample I, II and III derived from the profiles are approximately 73, 69 and 66 %, respectively.

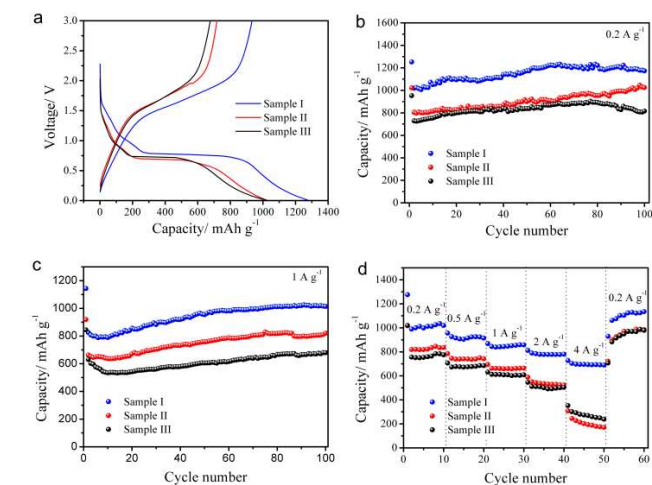


**Fig. 4** (a) First Discharge-charge curves of Sample I, II and III at  $0.2\text{ A g}^{-1}$ . (b, c) Cycling performances of Sample I, II and III at a current density of  $0.2\text{ A g}^{-1}$  or  $1.0\text{ A g}^{-1}$ . (d) Rate capability of the electrodes based on the branched core-shell  $\alpha\text{-Fe}_2\text{O}_3/\text{C}$  nanotubes with different thicknesses of the carbon layers.

The cycling stability of the electrodes based on Sample I, II, and III is also investigated at two current densities, 0.2 and 1.0 A g<sup>-1</sup>. As shown in Fig. 4b and 4c, all three samples display fair cycling performances, which might be related to the unique hollow feature, the uniform carbon coating and the large specific surface area from the branches. Among the three samples, it is still Sample I that shows the best cycling performances at both current densities. After 100 cycles at 0.2 and 1 A g<sup>-1</sup>, Sample I shows the specific capacities of 1173 and 1014 mAh g<sup>-1</sup>, respectively. The data are much higher than those of Sample II and III (Sample II: 1025 mAh g<sup>-1</sup> at 0.2 A g<sup>-1</sup> and 820 mAh g<sup>-1</sup> at 1 A g<sup>-1</sup>; Sample III: 815 mAh g<sup>-1</sup> at 0.2 A g<sup>-1</sup> and 680 mAh g<sup>-1</sup> at 1 A g<sup>-1</sup>.) The best electrochemical performance of Sample I probably come from the highest content of Fe<sub>2</sub>O<sub>3</sub> in the composite.

Fig. 4d shows the rate performances of Sample I, II and III tested at the current densities of 0.2, 0.5, 1, 2, 4 and 0.2 A g<sup>-1</sup>. Compared with Sample II and III, Sample I exhibits the best rate performances. It delivers the reversible specific capacities of 990, 926, 869 and 790 mAh g<sup>-1</sup> at the current densities of 0.2, 0.5, 1 and 2 A g<sup>-1</sup>. Even at a current density of 4 A g<sup>-1</sup>, a reversible capacity of 703 mAh g<sup>-1</sup> could be achieved, indicating the excellent rate capability. After the current density goes back to 0.2 A g<sup>-1</sup>, the specific capacity rebounds to 1062 mAh g<sup>-1</sup>, suggesting the good structure stability of the electrode at high rates. This is also confirmed by the SEM images of the electrode before and after cycling (Fig. S5). The good structure stability and superior rate capability of Sample I could be associated with the thin carbon layer in the composite that effectively inhibit the volume change during the discharge/charge processes, promote the electron conductivity between the electrolyte and the electrode (Fig. S6), and keep the carbon content low simultaneously. The high carbon content in the composite would greatly reduce the capacity of the entire electrode, because the theoretical capacity of carbon is far below that of Fe<sub>2</sub>O<sub>3</sub>. The rate capability of Sample I is also much better than those of well-designed Fe<sub>2</sub>O<sub>3</sub> nanomaterials. For example, hierarchical hollow spheres composed of ultrathin Fe<sub>2</sub>O<sub>3</sub> nanosheets presented a specific capacity of 540 mAh g<sup>-1</sup> at 2 A g<sup>-1</sup>.<sup>4</sup> After hybridized with graphene, the reversible capacity of Fe<sub>2</sub>O<sub>3</sub> nanoparticles increased to 624 mAh g<sup>-1</sup> at 2 A g<sup>-1</sup>.<sup>18</sup> But the encapsulation of Fe<sub>2</sub>O<sub>3</sub> nanoparticles in carbon nanotubes

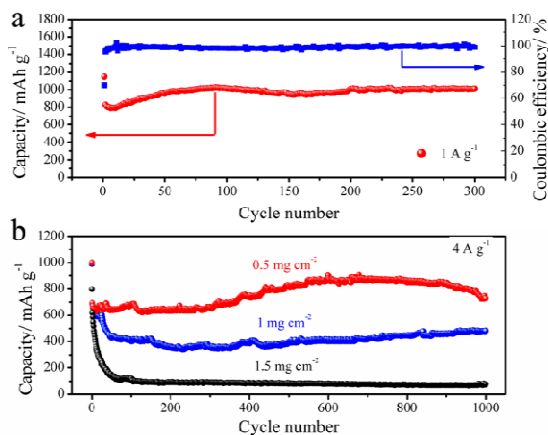


**Fig. 5** Long-term cycling performance of the branched core-shell  $\alpha$ -Fe<sub>2</sub>O<sub>3</sub>@C nanotubes (Sample I) at 1 A g<sup>-1</sup>(a) or 4 A g<sup>-1</sup> (b).

**Table 1** The cycling performances of some Fe<sub>2</sub>O<sub>3</sub> nanostructures.

Nanomaterials	Current density (mA g <sup>-1</sup> )	Cycle Number	Capacity (mAh g <sup>-1</sup> )
$\alpha$ -Fe <sub>2</sub> O <sub>3</sub> Nanoflakes <sup>27</sup>	65	80	~680
Flower-like $\alpha$ -Fe <sub>2</sub> O <sub>3</sub> <sup>33</sup>	100	10	929
$\alpha$ -Fe <sub>2</sub> O <sub>3</sub> Nanorods <sup>6</sup>	201	40	~900
$\alpha$ -Fe <sub>2</sub> O <sub>3</sub> Nanorod Arrays <sup>30</sup>	134	50	562
$\alpha$ -Fe <sub>2</sub> O <sub>3</sub> Hollow Spheres <sup>38</sup>	200	100	710
Mesoporous $\alpha$ -Fe <sub>2</sub> O <sub>3</sub> Nanoparticles <sup>34</sup>	200	50	1293
$\alpha$ -Fe <sub>2</sub> O <sub>3</sub> Nanotubes <sup>28</sup>	503	50	~1000
Hierarchical hollow Fe <sub>2</sub> O <sub>3</sub> spheres <sup>4</sup>	500	200	815
Fe <sub>2</sub> O <sub>3</sub> Nanoparticles in Carbon Nanotubes <sup>23</sup>	35	100	811
Graphene-Nanotube-Iron Nanostructure <sup>12</sup>	100	40	1024
Fe <sub>2</sub> O <sub>3</sub> @Polyaniline Hollow Spheres <sup>15</sup>	100	100	893
Polypyrrole-Coated Fe <sub>2</sub> O <sub>3</sub> @C <sup>43</sup>	200	100	785
Carbon-coated $\alpha$ -Fe <sub>2</sub> O <sub>3</sub> nanohorn on CNT <sup>22</sup>	500	100	800
Fe <sub>2</sub> O <sub>3</sub> -Graphene Nanocomposite <sup>44</sup>	1000	100	582
Our work	1000 4000	300 1000	1012 482

only exhibited a capacity of 335 mAh g<sup>-1</sup> at 1.2 A g<sup>-1</sup>.<sup>23</sup> Compared with this result, carbon-coated  $\alpha$ -Fe<sub>2</sub>O<sub>3</sub> hollow nanohorns on the carbon nanotubes gave a larger specific capacity of 420 mAh g<sup>-1</sup> even at 3 A g<sup>-1</sup>.<sup>22</sup> All these results are much lower than ours, which could be explained by the fact that the hierarchical core-shell nanotubes assemble all the strategies into one particle together.

Because the long-term cycling performance of the electrode at a high rate is highly desired for many practical applications, Sample I is further examined at 1 A g<sup>-1</sup> for 300 cycles and 4 A g<sup>-1</sup> for 1000 cycles. As presented in Fig. 5a, Sample I shows a reversible capacity of 1012 mAh g<sup>-1</sup> after 300 cycles. Meanwhile, it also exhibits a stable coulombic efficiency around 99 % except the first cycle, suggesting the good reversibility of the electrode during the lithiation/delithiation processes. The similar result is also obtained from the case at 4 A g<sup>-1</sup>. After 1000 cycles at 4 A g<sup>-1</sup>, Sample I delivers a specific capacity of 482 mAh g<sup>-1</sup>, as illustrated in Figure 5b. The data of the branched core-shell  $\alpha$ -Fe<sub>2</sub>O<sub>3</sub>@C nanotubes are much higher than most of the related reports, e.g. Fe<sub>2</sub>O<sub>3</sub> nanoflakes,<sup>27</sup> nanotubes,<sup>28</sup> nanorods,<sup>6, 29, 30</sup> flowers,<sup>31-33</sup> hollow/porous nanostructures<sup>4, 9, 11, 34-39</sup> and carbon coated/ supported nanostructures<sup>12, 15, 22, 23, 40-44</sup> (Table 1). The excellent performances of the branched core-shell nanotubes could be attributed to the synergistic effect of their hollow structure, carbon coating and branched surface, which effectively shorten the diffusion path of Li<sup>+</sup>, enhance the electrical conductivity and accommodate large volume changes.<sup>4, 45</sup> The above loading density of the active material is kept at ~1.0 mg cm<sup>-2</sup>. If the loading density of the active material increases to ~1.5 mg cm<sup>-2</sup>, the reversible capacity would greatly decrease to ~100 mAh g<sup>-1</sup> (Fig. 5b). But the reversible capacity could be also as high as 728 mAh g<sup>-1</sup> at a loading density of 0.5 mg cm<sup>-2</sup>. The

results demonstrate the important effect of the loading density of the active material on the lithium-storage performances.

## Conclusions

In summary, the branched core-shell  $\alpha$ -Fe<sub>2</sub>O<sub>3</sub>@C nanotubes have been synthesized by a facile hydrothermal reaction of the branched  $\beta$ -MnO<sub>2</sub>/ $\alpha$ -Fe<sub>2</sub>O<sub>3</sub> nanorods with glucose at 190 °C for 5 h. The obtained nanotubes inherit the size, shape and branch-structured surface from the  $\beta$ -MnO<sub>2</sub>/ $\alpha$ -Fe<sub>2</sub>O<sub>3</sub> nanorods. And the thickness of the carbon layer could be controlled by the ratio between  $\beta$ -MnO<sub>2</sub>/ $\alpha$ -Fe<sub>2</sub>O<sub>3</sub> nanorods and glucose. The branched core-shell  $\alpha$ -Fe<sub>2</sub>O<sub>3</sub>@C nanotubes with the carbon layer in different thicknesses are examined as an anode for LIBs. It is found that the nanotubes with a thinnest carbon layer show the best rate capability and cycling stability. They deliver a specific capacity of 1173 mAh g<sup>-1</sup> at 0.2 A g<sup>-1</sup> and 1014 mAh g<sup>-1</sup> at 1 A g<sup>-1</sup> after 100 cycles. Even after 300 cycles at 1 A g<sup>-1</sup> for or 1000 cycles at 4 A g<sup>-1</sup>, the specific capacity still could be maintained at 1012 or 482 mAh g<sup>-1</sup>, respectively. The result is attributed to the highest content of Fe<sub>2</sub>O<sub>3</sub> in the core-shell nanotubes with a thinnest carbon layer.

## Acknowledgements

This work was supported by the 973 Project of China (No. 2011CB935901), Natural Science Foundation of China (No.51172076, 21071055, 91022033, 21203111), New Century Excellent Talents in University (NCET-10-0369), Shandong Provincial Natural Science Foundation for Distinguished Young Scholar (JQ201205), New Faculty Start-up funding in Shandong University and Independent Innovation Foundations of Shandong University (2012ZD007). We want to thank Prof. Houyi Ma in Shandong University for helpful discussion.

## Notes and references

<sup>a</sup> Key Laboratory of Colloid and Interface Chemistry, Ministry of Education. School of Chemistry and Chemical Engineering, Shandong University, Jinan, 250100, P.R. China.

<sup>b</sup> E-mail: yangjian@sdu.edu.cn

<sup>c</sup> Hefei National Laboratory for Physical Science at Microscale, Department of Chemistry, University of Science and Technology of China, Hefei, 230026, P.R. China.

<sup>†</sup> Electronic Supplementary Information (ESI) available: XRD pattern and SEM image of  $\beta$ -MnO<sub>2</sub>/ $\alpha$ -Fe<sub>2</sub>O<sub>3</sub> nanorods, EDS spectra of core-shell  $\alpha$ -Fe<sub>2</sub>O<sub>3</sub>@C nanotubes, XRD pattern of  $\alpha$ -Fe<sub>2</sub>O<sub>3</sub> obtained from  $\alpha$ -Fe<sub>2</sub>O<sub>3</sub>@C nanotubes treated at 600 °C in air, SEM images of the electrode based on the branched core-shell  $\alpha$ -Fe<sub>2</sub>O<sub>3</sub>@C nanotubes before and after 10 cycles, Nyquist plots of the AC impedance spectra for the carbon-contained samples and carbon-free sample. See DOI: 10.1039/b000000x/

1. J. M. Tarascon and M. Armand, *Nature*, 2001, **414**, 359-367.
2. M. Armand and J. M. Tarascon, *Nature*, 2008, **451**, 652-657.
3. Y. Sun, X. Hu, W. Luo, F. Xia and Y. Huang, *Adv. Funct. Mater.*, 2013, **23**, 2436-2444.
4. J. Zhu, Z. Yin, D. Yang, T. Sun, H. Yu, H. E. Hoster, H. H. Hng, H. Zhang and Q. Yan, *Energy Environ. Sci.*, 2013, **6**, 987.
5. X. Wang, X.-L. Wu, Y.-G. Guo, Y. Zhong, X. Cao, Y. Ma and J. Yao, *Adv. Funct. Mater.*, 2010, **20**, 1680-1686.
6. Y.-M. Lin, P. R. Abel, A. Heller and C. B. Mullins, *J. Phys. Chem. Lett.*, 2011, **2**, 2885-2891.
7. S. Chaudhari and M. Srinivasan, *J. Mater. Chem.*, 2012, **22**, 23049.

8. X. Yao, C. Tang, G. Yuan, P. Cui, X. Xu and Z. Liu, *Electrochem. Commun.*, 2011, **13**, 1439-1442.
9. B. Koo, H. Xiong, M. D. Slater, V. B. Prakapenka, M. Balasubramanian, P. Podsiadlo, C. S. Johnson, T. Rajh and E. V. Shevchenko, *Nano Lett.*, 2012, **12**, 2429-2435.
10. J. Chen, L. Xu, W. Li and X. Gou, *Adv. Mater.*, 2005, **17**, 582-586.
11. Z. Wu, K. Yu, S. Zhang and Y. Xie, *J. Phys. Chem. C*, 2008, **112**, 11307-11313.
12. S.-H. Lee, V. Sridhar, J.-H. Jung, K. Karthikeyan, Y.-S. Lee, R. Mukherjee, N. Koratkar and I.-K. Oh, *ACS Nano*, 2013, **7**, 4242-4251.
13. A. Brandt and A. Balducci, *J. Power Sources*, 2013, **230**, 44-49.
14. Q. Zhu, N. Chen, F. Tao and Q. Pan, *J. Mater. Chem.*, 2012, **22**, 15894.
15. J. M. Jeong, B. G. Choi, S. C. Lee, K. G. Lee, S. J. Chang, Y. K. Han, Y. B. Lee, H. U. Lee, S. Kwon, G. Lee, C. S. Lee and Y. S. Huh, *Adv. Mater.*, DOI: 10.1002/adma.201302710.
16. J. Luo, X. Xia, Y. Luo, C. Guan, J. Liu, X. Qi, C. F. Ng, T. Yu, H. Zhang and H. J. Fan, *Adv. Energy Mater.*, 2013, **3**, 737-743.
17. Y. Luo, J. Luo, J. Jiang, W. Zhou, H. Yang, X. Qi, H. Zhang, H. J. Fan, D. Y. W. Yu, C. M. Li and T. Yu, *Energy Environ. Sci.*, 2012, **5**, 6559.
18. L. Xiao, D. Wu, S. Han, Y. Huang, S. Li, M. He, F. Zhang and X. Feng, *ACS Appl. Mater. Interfaces*, 2013, **5**, 3764-3769.
19. J. Ma, X. Zhang, K. Chen, G. Li and X. Han, *J. Mater. Chem. A*, 2013, **1**, 5545.
20. W. Zhang, Y. Zeng, N. Xiao, H. H. Hng and Q. Yan, *J. Mater. Chem.*, 2012, **22**, 8455.
21. L. Chen, H. Xu, L. e. Li, F. Wu, J. Yang and Y. Qian, *J. Power Sources*, 2014, **245**, 429-435.
22. Z. Wang, D. Luan, S. Madhavi, Y. Hu and X. W. Lou, *Energy Environ. Sci.*, 2012, **5**, 5252.
23. W.-J. Yu, P.-X. Hou, F. Li and C. Liu, *J. Mater. Chem.*, 2012, **22**, 13756.
24. X. Gu, L. Chen, Z. Ju, H. Xu, J. Yang and Y. Qian, *Adv. Funct. Mater.*, 2013, **23**, 4049-4056.
25. L. Zhang, G. Zhang, H. B. Wu, L. Yu and X. W. D. Lou, *Adv. Mater.*, 2013, **25**, 2589-2593.
26. X.-L. Wu, Y.-G. Guo, L.-J. Wan and C.-W. Hu, *J. Phys. Chem. C*, 2008, **112**, 16824-16829.
27. M. V. Reddy, T. Yu, C. H. Sow, Z. X. Shen, C. T. Lim, G. V. SubbaRao and B. V. R. Chowdari, *Adv. Funct. Mater.*, 2007, **17**, 2792-2799.
28. Z. Wang, D. Luan, S. Madhavi, C. M. Li and X. W. Lou, *Chem. Commun.*, 2011, **47**, 8061-8063.
29. C. Wu, P. Yin, X. Zhu, C. OuYang and Y. Xie, *J. Phys. Chem. B*, 2006, **110**, 17806-17812.
30. Y. Song, S. Qin, Y. Zhang, W. Gao and J. Liu, *J. Phys. Chem. C*, 2010, **114**, 21158-21164.
31. Y. NuLi, P. Zhang, Z. Guo, P. Munroe and H. Liu, *Electrochim. Acta*, 2008, **53**, 4213-4218.
32. S. Zeng, K. Tang, T. Li, Z. Liang, D. Wang, Y. Wang, Y. Qi and W. Zhou, *J. Phys. Chem. C*, 2008, **112**, 4836-4843.
33. Y. Han, Y. Wang, L. Li, Y. Wang, L. Jiao, H. Yuan and S. Liu, *Electrochim. Acta*, 2011, **56**, 3175-3181.
34. B. Sun, J. Horvat, H. S. Kim, W.-S. Kim, J. Ahn and G. Wang, *J. Phys. Chem. C*, 2010, **114**, 18753-18761.
35. S. Zeng, K. Tang, T. Li, Z. Liang, D. Wang, Y. Wang and W. Zhou, *J. Phys. Chem. C*, 2007, **111**, 10217-10225.
36. J. Zhou, H. Song, X. Chen, L. Zhi, S. Yang, J. Huo and W. Yang, *Chem. Mater.*, 2009, **21**, 2935-2940.
37. H. S. Kim, Y. Piao, S. H. Kang, T. Hyeon and Y.-E. Sung, *Electrochem. Commun.*, 2010, **12**, 382-385.
38. B. Wang, J. S. Chen, H. B. Wu, Z. Wang and X. W. Lou, *J. Am. Chem. Soc.*, 2011, **133**, 17146-17148.
39. X. Xu, R. Cao, S. Jeong and J. Cho, *Nano Lett.*, 2012, **12**, 4988-4991.
40. W. J. Yu, P. X. Hou, L. L. Zhang, F. Li, C. Liu and H. M. Cheng, *Chem. Commun.*, 2010, **46**, 8576-8578.
41. Y. Zhao, J. Li, Y. Ding and L. Guan, *Chem. Commun.*, 2011, **47**, 7416-7418.

- 
42. W. Zhou, J. Zhu, C. Cheng, J. Liu, H. Yang, C. Cong, C. Guan, X. Jia, H. J. Fan, Q. Yan, C. M. Li and T. Yu, *Energy Environ. Sci.*, 2011, **4**, 4954.
43. F. Han, D. Li, W.-C. Li, C. Lei, Q. Sun and A.-H. Lu, *Adv. Funct. Mater.*, 2013, **23**, 1692-1700.
44. Y. Zou, J. Kan and Y. Wang, *J. Phys. Chem. C*, 2011, **115**, 20747-20753.
45. J. Jiang, Y. Li, J. Liu, X. Huang, C. Yuan and X. W. Lou, *Adv. Mater.*, 2012, **24**, 5166-5180.

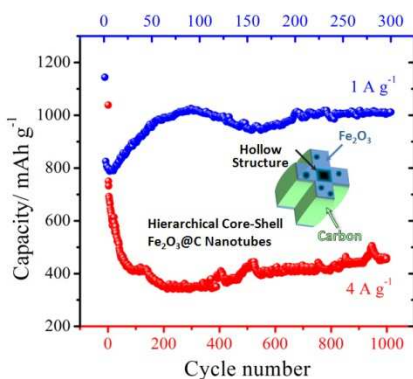
10

*Table of Content***Hierarchical Core-Shell  $\alpha$ -Fe<sub>2</sub>O<sub>3</sub>@C Nanotubes as a High-Rate and Long-life Anode for Advanced Lithium Ion Batteries**

5 Xin Gu,<sup>a</sup> Liang Chen,<sup>a</sup> Shuo Liu,<sup>a</sup> Huayun Xu,<sup>a</sup> Jian Yang\*<sup>a</sup>, and Yitai Qian<sup>ab</sup>

[a] Key Laboratory of Colloid and Interface Chemistry, Ministry of Education. School of Chemistry and Chemical Engineering, Shandong University, Jinan, 250100, P.R. China.  
E-mail: yangjian@sdu.edu.cn

[b] Hefei National Laboratory for Physical Science at Microscale. Department of Chemistry, University of Science and Technology of  
10 China, Hefei, 230026, P.R. China



Hierarchical core-shell  $\alpha$ -Fe<sub>2</sub>O<sub>3</sub>@C nanotubes prepared by a mild hydrothermal reaction, presented an excellent cycling stability and rate capability for lithium ion batteries.